IEEE Access
Multidisciplinary | Rapid Review | Open Access Journal

Received October 1, 2017, accepted November 22, 2017, date of publication November 29, 2017, date of current version March 9, 2018.

Digital Object Identifier 10.1109/ACCESS.2017.2778270

Air Core Transformer Winding Disk Deformation: A Precise Study on Mutual Inductance Variation and Its Influence on Frequency Response Spectrum

MEHDI BAGHERI[1], (Member, IEEE), SVYATOSLAV NEZHIVENKO[1], B. T. PHUNG[2], (Senior Member, IEEE), AND TREVOR BLACKBURN[2]

[1]Department of Electrical and Computer Engineering, Nazarbayev University, Astana 010000, Kazakhstan
[2]School of Electrical Engineering and Telecommunications, University of New South Wales, Sydney, NSW 2052, Australia

Corresponding author: Mehdi Bagheri (mehdi.bagheri@nu.edu.kz)

ABSTRACT It is well-known that the deformation of transformer winding can produce detectable changes to the frequency response spectrum compared with a referenced past measurement. To interpret such changes for diagnostic purposes, main causes of the trace deviation need to be recognized precisely. In addition, it is useful that the interpretation of transformer frequency response is classified in a way that IoT-based techniques can be developed in the near future to analyze the transformer mechanical integrity. This paper has specifically concentrated on the inductance and capacitance variation due to the axial and radial disk deformation of transformer winding. Analytical analyses on self- and mutual-inductance variations are discussed and capacitance variation is studied in detail for symmetrical and asymmetrical transformer disk deformations. A numerical example is provided to establish the analytical approach and compare inductance and capacitance variation. The analytical approach is finally examined through the experimental study of disk deformation in a 66 kV transformer winding.

INDEX TERMS Axial deformation, frequency response analysis, radial deformation, transformer winding deformation.

NOMENCLATURE

L_{eq}	Elemental inductance matrix of winding
L_A	Elemental inductance matrix of disk (disk A)
M_{AB}	Elemental mutual inductance of disks A and B
L_1	Turn inductance value (scalar value)
M_{12}	Turn-to-turn mutual inductance between turns 1 and 2 (scalar value)
L_{A-disc}	Equivalent inductance of disk A, summation of all arrays in L_A (scalar value)
M_{A-disc}	Equivalent mutual inductance of the first disk, summation of all arrays in M_{AB} (scalar value)
L_{eq-w}	Equivalent self-inductance of multi-section lumping (winding), summation of all arrays in L_{eq} (scalar value)
M_{eq-w}	Equivalent mutual inductance of multi-section lumping (winding), summation of mutual arrays in L_{eq} (scalar value)
L	Self-inductance of an air-core circular disk (scalar value)
N	Number of turns within a disk
R	Mean radius of a disk
h	Axial dimension of conductor
W	Radial dimension of the winding cross section
M	Turn-to-turn mutual inductance
R_a, R_b	Mean radius of the turns a and b
M_{xy}	Mutual inductance between turns x and y
U	Voltage drop across the pair of disks
C_t	Total turn-to-turn capacitance of a pair-disk
C_{tt}	Turn-to-turn capacitance
C_d	Total disk-to-disk capacitance of a pair-disk
C_{dd}	Scattered disk-to-disk capacitance
δ_t	Thickness of inter-turn insulation
ε_t	Relative permittivity of paper insulation
ε_0	Vacuum permittivity
n	Turn number

2169-3536 © 2017 IEEE. Translations and content mining are permitted for academic research only.
Personal use is also permitted, but republication/redistribution requires IEEE permission.
See http://www.ieee.org/publications_standards/publications/rights/index.html for more information.

l	Total length of conductor in one disk
C_s	Equivalent series capacitance of winding
C_{s-pair}	Equivalent series capacitance of pair-disk
C_g	Winding shunt capacitance
H	Height of the winding
r_1	Mean radius value of winding
r_2	Mean radius value of circular tank
M'	Mutual inductance of circular filaments whose axes are inclined
X	Maximum axial displacement of the outermost turn from the origin
d	Mean turn-to-turn distance
M''	Mutual inductance between the turns for asymmetrical axial deformation
C'_{tt}	Turn to turn capacitance in a deformed disk
η	Ratio of entire trigonometric circular span (2π) over the deformation span (rad)
δ_d	Disk-to-disk distance
r'	Radial deformation radius
ϕ_b	Induced magnetizing flux on the second loop due to the current initiated by the first loop
I_a	Current flowing through conductor a
μ_0	Vacuum permeability

I. INTRODUCTION

Frequency Response Analysis (FRA) has been in use as a comparative diagnosis method for several years, and its accuracy and sensitivity have been extensively discussed in the literatures [1]–[5]. Initial FRA measurements during factory testing are taken as the winding fingerprint (reference) [6]. Any subsequent changes in winding structural configuration would almost certainly cause changes in the frequency response trace [7], [8]. Although this method has been applied in industry since the last decade, accurate interpretation of the FRA trace is still very much under development. The FRA trace is commonly presented as Bode diagrams, with frequency on the x-axis and the response magnitude on the y-axis. Self- and mutual inductance or series- and shunt-capacitance variation will cause some changes to the FRA trace [9].

In [10], it is concluded that ''the changes of capacitance can be neglected in the model for axial displacement studies and the changes in inductance matrix can be neglected for the radial deformation study''. Another study by researchers in [11] asserted that inductance and capacitance would change following axial movement of the winding. Recent literatures also have discussed on axial and radial deformations in transformer winding. Classification of transformer winding faults using a new calculation method is also recommend in [12]. Although a numbers of studies have been conducted on FRA trace deviation due to the winding parameter variation, there is still considerable ambiguity on how winding parameters are changed under such structural movements.

Nowadays, available powerful numerical methods such as finite element provide the ability to calculate distributed parameters in transformer winding precisely. However, it would be of interest to address the problem through analytical methods as this approach can assist in the physical understanding and may also help in automated prognosis algorithm design for cloud computing.

In order to gain new knowledge on FRA trace interpretation through analytical approach, this study has specifically focused on inductance and capacitance variation due to the axial and radial deformation in an air-core transformer winding disk.

To conduct the study, an air-core continuous disk winding having four disks and four conductor turns in each disk is proposed as a model. It is also assumed that the model winding is enclosed in a cylindrical metal tank. At first, the self- and mutual inductances as well as series and shunt capacitances are calculated for the winding in normal (not deformed) condition. Afterwards, one of the winding disks is supposed to be deformed axially and the resultant changes in parameters are analyzed, analytically. This step is carried out for symmetrical as well as asymmetrical axial deformations. Then, radial deformation of the winding is modeled through buckling and all parameters are calculated and discussed. This stage is also studied through computer simulations using 3D finite element and the results are compared with those obtained from the analytical approach. It should be highlighted that the case of inductance calculation has been quite thoroughly treated through a number of major studies. Formulas for circular filaments were first given by Maxwell [13]. Subsequently, Rayleigh [14], Lyle [15], Butterworth [16], Snow [17], Rosa [18], Curtis and Sparks [19], Grover [20], Babic *et al.* [21], Conway [22], etc., have developed and derived others formulas and tables to calculate self and mutual inductances.

In this study, the Grover's equation [20] is used for the self-inductance calculation of circular coils of rectangular cross section as well as mutual inductance calculation for coaxial circular filaments. Grover's formulas are then developed for the calculation of transformer winding inductance matrix for the case of axial and radial deformation. It should be noted that to simplify inductance calculations, the thickness of paper insulation wrapped over the conductors is ignored in this study, but for capacitance calculation this thickness is taken into consideration. At the end, a numerical example using the analytical approach is provided. Self and mutual inductances as well as series and shunt capacitances are calculated in detail for axial and radial deformation. The results are compared and deviation in each parameter is discussed. This is followed with measurement results from a practical study on a deformed winding to examine the analytical approach.

In general, this paper is structured as follows: (1) analytical discussion on inductance and capacitance variation in axial and radial deformation with focus mainly on mutual inductance changes, sections III, IV, and V; (2) numerical example to find changes of inductance in axial tilting of transformer winding disk and simulation on radial deformation of

winding disk, section VI; (3) a practical study and emulation of transformer winding disk tilting on an isolated 66 kV transformer winding, section VII.

II. PROPOSED WINDING AND ITS PARAMETERS

In the absence of magnetic materials, self and mutual inductances are parameters dependent only on the geometric size/location of the winding conductors and are independent of the current [20]. Hence, to study the influence of axial and radial deformation on distributed parameters of transformer winding, an air-core model is proposed and shown in Fig. 1. The winding has four disks and four conductor turns per disk.

A. TRANSFORMER WINDING INDUCTANCE

1) ANALYTICAL ANALYSIS

The elemental inductance matrix of the winding illustrated in Fig. 1 is given by (1), as shown at the bottom of this page, in general form and (2), as shown at the bottom of this page, in detailed form:

where,

$$L_A = \begin{bmatrix} L_1 & M_{12} & M_{13} & M_{14} \\ M_{21} & L_2 & M_{23} & M_{24} \\ M_{31} & M_{32} & L_3 & M_{34} \\ M_{41} & M_{42} & M_{43} & L_4 \end{bmatrix},$$

$$M_{AB} = \begin{bmatrix} M_{15} & M_{16} & M_{17} & M_{18} \\ M_{25} & M_{26} & M_{27} & M_{28} \\ M_{35} & M_{36} & M_{37} & M_{38} \\ M_{45} & M_{46} & M_{47} & M_{48} \end{bmatrix}, \ldots \quad (3)$$

In the above, L_A is the elemental inductance matrix of disk A, M_{AB} is the elemental mutual inductance matrix of disks A and B, L_1 denotes the turn inductance, and M_{12} is the turn-to-turn mutual inductance between turns 1 and 2.

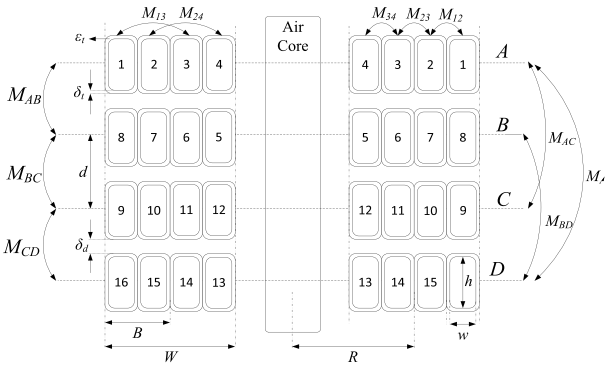

FIGURE 1. Air-core transformer winding model. Disks *A* and *C* assumed as normally wound, and Disks *B* and *D* reversely wound.

Kirchhoff [23] has shown that the equivalent self-inductance of a disk is equal to the summation of the self- and the mutual inductance of each turn with respect to all the other turns in that disk. Hence, for the proposed winding, the equivalent inductance of the section lumped together for the first disk (L_{A-disc}) is given by (4) while the equivalent mutual inductance of the same disk is given by (5):

$$L_{A-disc} = L_1+L_2+L_3+L_4+2\begin{pmatrix} M_{12}+M_{13}+M_{23} \\ +M_{14}+M_{24}+M_{34} \end{pmatrix} \quad (4)$$

$$M_{A-disc} = 2\left(M_{12}+M_{13}+M_{23}+M_{14}+M_{24}+M_{34}\right) \quad (5)$$

Equations (4) and (5) will be utilized later to compare the mutual inductance variation in a disk due to axial deformation of the winding. These equations can be extended for any number of disks and not restricted to a single disk; hence, using the summation method on a single section lump, the

$$L_{eq} = \begin{bmatrix} L_A & M_{AB} & M_{AC} & M_{AD} \\ M_{BA} & L_B & M_{BC} & M_{BD} \\ M_{CA} & M_{CB} & L_C & M_{CD} \\ M_{DA} & M_{DB} & M_{DC} & L_D \end{bmatrix} \quad (1)$$

$$= \begin{bmatrix} L_1 & M_{12} & M_{13} & M_{14} & M_{15} & M_{16} & M_{17} & M_{18} & M_{19} & M_{110} & M_{111} & M_{112} & M_{113} & M_{114} & M_{115} & M_{116} \\ . & L_2 & M_{23} & M_{24} & M_{25} & M_{26} & M_{27} & M_{28} & M_{29} & M_{210} & M_{211} & M_{212} & M_{213} & M_{214} & M_{215} & M_{216} \\ . & . & L_3 & M_{34} & M_{35} & M_{36} & M_{37} & M_{38} & M_{39} & M_{310} & M_{311} & M_{312} & M_{313} & M_{314} & M_{315} & M_{316} \\ . & . & . & L_4 & M_{45} & M_{46} & M_{47} & M_{48} & M_{49} & M_{410} & M_{411} & M_{412} & M_{413} & M_{414} & M_{415} & M_{416} \\ . & . & . & . & L_5 & M_{56} & M_{57} & M_{58} & M_{59} & M_{510} & M_{511} & M_{512} & M_{513} & M_{514} & M_{515} & M_{516} \\ . & . & . & . & . & L_6 & M_{67} & M_{68} & M_{69} & M_{610} & M_{611} & M_{612} & M_{613} & M_{614} & M_{615} & M_{616} \\ . & . & . & . & . & . & L_7 & M_{78} & M_{79} & M_{710} & M_{711} & M_{712} & M_{713} & M_{714} & M_{715} & M_{716} \\ . & . & . & . & . & . & . & L_8 & M_{89} & M_{810} & M_{811} & M_{812} & M_{813} & M_{814} & M_{815} & M_{816} \\ . & . & . & . & . & . & . & . & L_9 & M_{910} & M_{911} & M_{912} & M_{913} & M_{914} & M_{915} & M_{916} \\ . & . & . & . & . & . & . & . & . & L_{10} & M_{1011} & M_{1012} & M_{1013} & M_{1014} & M_{1015} & M_{1016} \\ . & . & . & . & . & . & . & . & . & . & L_{11} & M_{1112} & M_{1113} & M_{1114} & M_{1115} & M_{1116} \\ . & . & . & . & . & . & . & . & . & . & . & L_{12} & M_{1213} & M_{1214} & M_{1215} & M_{1216} \\ . & . & . & . & . & . & . & . & . & . & . & . & L_{13} & M_{1314} & M_{1315} & M_{1316} \\ . & . & . & . & . & . & . & . & . & . & . & . & . & L_{14} & M_{1415} & M_{1416} \\ . & . & . & . & . & . & . & . & . & . & . & . & . & . & L_{15} & M_{1516} \\ . & . & . & . & . & . & . & . & . & . & . & . & . & . & . & L_{16} \end{bmatrix} \quad (2)$$

elemental inductance matrix (L_{eq}), equivalent self-inductance for multi-section lumping (winding) of Fig.1 is given as:

$$L_{eq-w} = L_{A-disc} + L_{B-disc} + L_{C-disc} + L_{D-disc} + 2\begin{pmatrix} M_{AB} + M_{AC} + M_{BC} \\ + M_{AD} + M_{BD} + M_{CD} \end{pmatrix} \quad (6)$$

The mutual inductance of the winding, M_{eq-w}, is then defined as:

$$M_{eq-w} = 2\left(M_{AB} + M_{AC} + M_{BC} + M_{AD} + M_{BD} + M_{CD}\right) \quad (7)$$

It should be clarified that similar to L_{A-disc}; $M_{AB}, M_{AC}, \ldots$ are equivalent mutual inductance of the other disks lumped together and they are scalar values. It also should be noted that (2) is a symmetric matrix for any winding configurations. It will be shown later that this matrix will change once axial deformation occurs.

2) Calculation

a: SELF-INDUCTANCE

The self-inductance of a circular winding with a rectangular cross section is a function of winding shape. The significant parameters defining the winding shape are the mean radius of the turns per disks, and axial and radial dimensions of the conductor cross section. These parameters are illustrated in Fig. 1. Based on this, the self-inductance (L) of an air-core circular disk for $h = W$ is given by [20]:

$$L = 0.001RN^2P_0 \quad \mu H \quad (8)$$

where, N is the number of turns within a disk, R is the mean radius of disk's turns, h is the axial dimension of the conductor cross section, W is the radial dimension of the winding cross section, and P_0 is a function of $W/2R$. For relatively small cross sections category such that ($W/2R < 0.2$), P_0 is given by [20]:

$$P_0 = 4\pi\left(\begin{pmatrix}\frac{1}{2} + \frac{1}{12}\left(\frac{W}{2R}\right)^2\end{pmatrix}\ln\left(8\left(\frac{2R}{W}\right)^2\right) - 0.84834 + 0.2041\left(\frac{W}{2R}\right)^2\right) \quad (9)$$

For a thin circular disk with rectangular cross section of any desired proportions ($h \neq W$), the self-inductance is given by:

$$L = 0.019739\left(\frac{2R}{W}\right)N^2R(K - k_0) \quad \mu H \quad (10)$$

where K comes through Nagaoka's formula [24] and can be derived through Table 2 in the Appendix I, and k_0 is a factor that specifies circular inductance decrement due to the separation of turns in radial direction. For a single turn with significant mean radius dimension, k_0 could be zero. It should be noted that L in (8) and (10) would be almost equal to the value obtained in (3). Indeed, Grover has tried to bring the extensive disk inductance calculation in (3) into a single lumped form in (8) or (10).

b: MUTUAL INDUCTANCE

The mutual inductance of a transformer winding can be calculated for one disk with respect to another disk as given by (11):

$$M_{XY} = N_1N_2M_0, \quad \mu H \quad (11)$$

or it can be achieved through summation of the turn-to-turn mutual-inductances as obtained by (7). In this equation, N_1 and N_2 denote the number of turns of different disks, and M_0 is calculated using Lyle's method [15].

In our study, as the main goal is specifically focused on turn-to-turn mutual-inductance variation in axial and radial winding deformation, we focus on turn by turn mutual-inductance analytical calculation and then collect them to find the entire mutual inductance in matrix form. The mutual-inductance of coaxial circular filaments is given by [25]:

$$M = f\sqrt{R_bR_a} \quad \mu H \quad (12)$$

where M denotes each and every turn mutual inductance as illustrated in (3), (for instance M_{12}, $M_{13}, \ldots$). R_a and R_b are the mean radius of the turns a and b, respectively (see Fig. 2(a)). f is a function of parameter k which is given by:

$$k = \frac{(1-\alpha)^2 + \beta^2}{(1+\alpha)^2 + \beta^2}, \quad \alpha = \frac{R_a}{R_b}, \quad \beta = \frac{d}{R_b} \quad (13)$$

d is the distance between the circular turns as illustrated in Fig. 2. For a typical transformer winding, $k \leq 0.1$; thus, f can be obtained by [20]:

$$f = 0.014468\left(\log_{10}\frac{1}{k} - 0.53307\right) \quad (14)$$

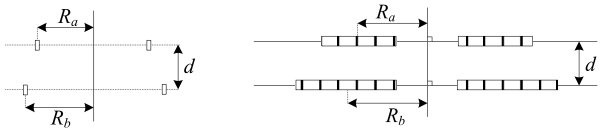

FIGURE 2. Coaxial circular filaments, (a) two coaxial filaments, (b) several circular filaments in a transformer disk form.

For the inter-turn mutual inductance between two conductors in a common disk $\beta = 0$; and for the inter-disk mutual inductances of the conductors in different disks with equal mean radii, $\alpha = 1$ can be taken into consideration. Therefore, all mutual inductances (M_{xy}) in (2) can be obtained one by one using (12).

B. TRANSFORMER WINDING CAPACITANCE

1) SERIES CAPACITANCE

To calculate the equivalent series capacitance in a continuous disk winding, the energy summation method is used. According to this method, the summation of energies in the capacitances along a pair of disks is equal to the total energy which exists within those two disks. It is assumed that the number of conductor turns in each disk is N. The number of

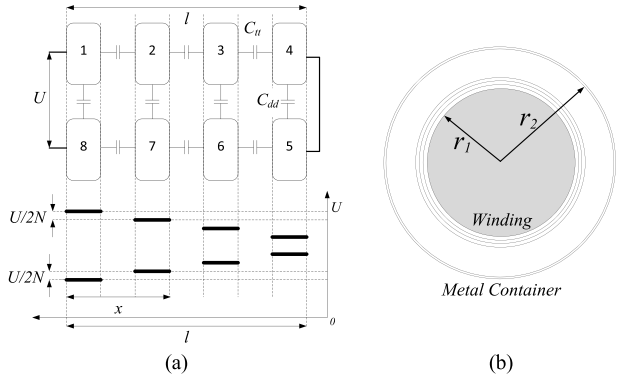

FIGURE 3. Pair of disks, (a) Cross-section overview and voltage distribution along pair disks, (b) Up side view of the proposed winding including metal container.

series capacitors between turns, as shown in Fig. 3, will be $2N-2$ for a pair of disks. Therefore, the total equivalent capacitance between the conductors (C_t) is given by [26]:

$$\frac{1}{2}C_t U^2 = (2N-2)\frac{1}{2}C_{tt}\left(\frac{U}{2N}\right)^2,\ C_t = \frac{1}{2}C_{tt}\left(\frac{N-1}{N^2}\right) \tag{15}$$

where U is the voltage drop across a pair of disks, see Fig. 3(a), and C_{tt} is given by:

$$C_{tt} = \varepsilon_t \varepsilon_0 R\pi\left(\frac{h+2\delta_t}{2\delta_t}\right) \tag{16}$$

where δ_t is the thickness of inter-turn insulation, ε_t is the relative permittivity of paper insulation, and ε_0 is the vacuum permittivity.

Calculation of the equivalent inter-disk capacitance (C_d) is based on the voltage distribution demonstrated in Fig. 3(a).

According to Fig. 3(a), when moving from end points starting from conductor number 1 or number 8 towards the middle of the winding (conductor number 4 and number 5), the voltage on corresponding conductors will change in a non-linear manner along the pair of disk. Hence, the steady state voltage distributions for conductors in the upper and lower disks are as follows:

$$U_{up}(n) = U\frac{2l-x}{2l},\quad U_{down}(n) = U\frac{x}{2l} \tag{17}$$

where n is the turn number and l is the total length of conductor in one disk. The equivalent capacitance between two disks is then obtained as [26]:

$$\frac{1}{2}C_d U^2 = \frac{1}{2}C_{dd}(U_{up}(n)-U_{down}(n))^2,\quad C_d = \frac{C_{dd}}{3}l \tag{18}$$

The summation of C_t and C_d gives the equivalent series capacitance C_{s-pair} for a pair of disks in a continuous disk winding:

$$C_{s-pair} = C_d + C_t \tag{19}$$

The first part in (19) is related to the capacitances between the disks, and the second part is related to the capacitances between the conductors. The equivalent series capacitance for the entire winding (C_s) is then obtained by:

$$C_s = \frac{1}{N_d}\left(4\frac{N_d-1}{N_d}C_d + \frac{(N_w/N_d)-1}{(N_w/N_d)^2}C_{tt}\right) \tag{20}$$

where N_d is the number of transformer winding discs, and N_w is the number of winding turns.

2) SHUNT CAPACITANCE

Referring to Fig. 3(b), the shunt capacitance between the winding and the cylindrical metal container (tank) is given by:

$$C_g = \frac{2\pi H\varepsilon_0}{\ln(r_2/r_1)} \tag{21}$$

where, H is the height of the winding, r_1 is the radial dimension of the winding, r_2 denotes the radial dimension of the tank, and δ_t as compared to r_2 is ignored.

III. AXIAL DEFORMATION OF WINDING DISK AND ITS IMPACTS ON WINDING PARAMETERS

Axial or radial deformation or displacement in transformer winding may be due to short circuit currents, earthquakes, careless transportation between sites, explosion of combustible gases accumulating in the transformer oil, etc.

A. MUTUAL INDUCTANCE OF CIRCULAR FILAMENTS WHOSE AXES INCLINED TO ONE ANOTHER

It is possible for axial deformation to occur symmetrically or asymmetrically for one or several disks. This work is specifically concerned with symmetrical and asymmetrical axial deformation of a disk among four disks as illustrated in Figures 4 and 5. Figures 4(a) and 5(a) show the deformation patterns, whereas Figures 4(b) and 5(b) illustrate their implementation in the winding.

1) SYMMETRICAL AXIAL DEFORMATION OF A DISK

The mutual inductance of the circular filaments whose axes are inclined to one another is given by [25]:

$$M' = R_0 M\cos\theta = R_0 f\sqrt{R_b R_a}\cos\theta\quad \mu H \tag{22}$$

where, M is calculated as (12), and R_0 is a function of θ and given by:

where, X is the maximum axial displacement of the outermost turn from the origin. The formulas for $P_m(\mu)$ and $P'_m(\nu)$ are provided through (A1) and (A2) in the Appendix I [13]. In the case of a transformer winding, parameter α generally takes a value between 0.6 and 0.9 (due to typical radius of innermost and outermost conductors in a disk, $0.6R_b < R_a < 0.9R_b$). Hence for convenience, in the range of $0.6 < \alpha < 0.9$ some of pre-calculated values of R_0 are provided in Table 3 in the Appendix.

Based on Table 3, R_0 is a value less than 1 for a typical transformer winding. In addition, $cos\theta \leq 1$; hence, $M' \leq M$. Therefore, the mutual inductances between the winding turns for the symmetrical deformation of a disk show smaller

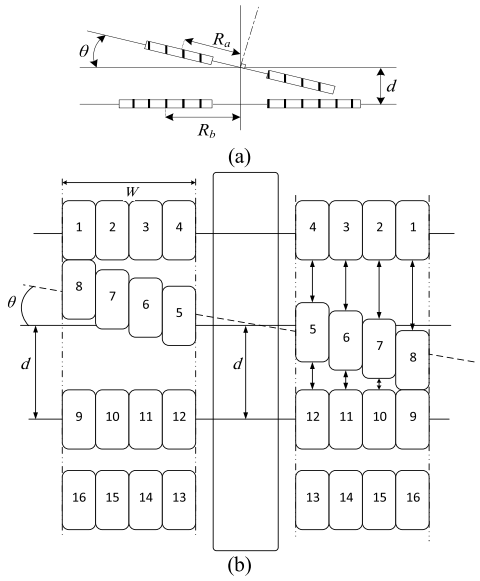

FIGURE 4. Symmetrical axial deformation of a disk, (a) Axial deformation pattern, (b) Deformed disk.

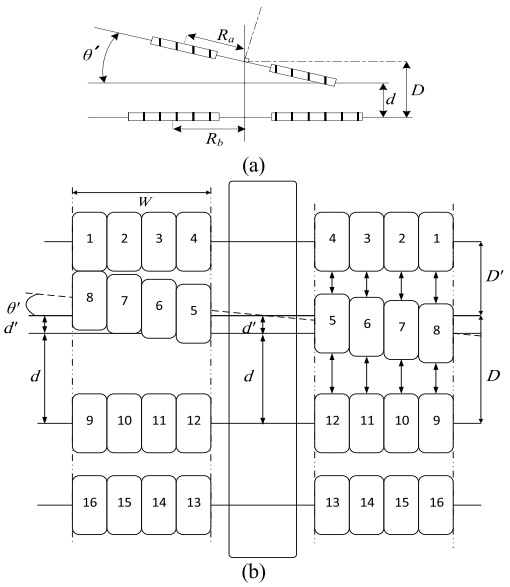

FIGURE 5. Asymmetrical axial deformation of a disk, (a) Axial deformation pattern, (b) Deformed disk, *d* is the center to center distance between the second and third disks in normal condition as well as symmetrical deformation, and *D* denotes the center to center distance between the second and third disks in asymmetrical deformation.

values as compared to the normal winding. This in turn influences very little the total self-inductance of the winding.

2) ASYMMETRICAL AXIAL DEFORMATION OF A DISK

The mutual inductance between the turns for asymmetrical axial deformation of a disk is given by:

$$M'' = R_0 M_a \cos\theta' = R_0 f'' \sqrt{R_b R_a}\cos\theta' \quad \mu H \tag{24}$$

According to Fig. 5, the distance between the second and third disks has been changed from d to D, while $D > d$. Hence, β in (13) should be replaced by β_{down} for mutual inductance calculation between the turns in the second and third disks, and given as follows:

$$\beta_{down} = \frac{D}{R_b} = \frac{d + R_a \sin\theta'}{R_b} \tag{25}$$

β_{up} is then defined as (26) and represents the ratio of the distance between the first and second disks and R_b,

$$\beta_{up} = \frac{D'}{R_b} = \frac{d - R_a \sin\theta'}{R_b} \tag{26}$$

Other parameters in (23), as shown at the bottom of this page, should also be replaced by:

$$\kappa'^2 = \frac{\alpha^2}{1+\beta_x^2}, \quad \nu'^2 = \frac{\beta_x^2}{1+\beta_x^2},$$
$$\theta' = \sin^{-1}\left(\frac{X}{2R_a}\right), \quad \mu' = \cos\theta' \tag{27}$$

where, β_x can take β_{down} or β_{up} in (27) for the mutual inductance calculation of the second disk with respect to the third or first disk, respectively. In addition, μ can be replaced by μ', κ^2 by κ'^2, and ν^2 by ν'^2 in (23) and k by k_{down} or k_{up} in (13) and (14), accordingly.

Since $\beta_{up} < \beta < \beta_{down}$, therefore, $k_{up} < k < k_{down}$ and $f_{up} > f > f_{down}$. Hence, we define $A_1 = f_{up} - f > 0$, and $A_2 = f_{down} - f < 0$. Based on (14), if $f_{down} < f_{up}$ then $|A_1| > |A_2|$ and eventually the total value of f'' for asymmetrical deformation would be less than the mutual inductance coefficient, f, in the normal winding. This factor causes M'' to experience a larger value than M.

On the other hand, as discussed earlier, R_0 is a value less than 1 for a routine normal transformer winding. In addition, $\cos\theta'$ is ≤ 1. Hence, M'' can take a value less than M. Therefore, two factors ($\cos\theta$ and R_0) will decrease the value of M'' and one factor (f'') can increase it. Thus, it is difficult to confirm analytically the magnitude of M'' as compared to M. In order to determine which factors are more significant in changing their relative magnitude, a numerical example is provided in the next subsections and the results are discussed to clarify this point.

$$R_0 = \frac{1 - \frac{1}{4}\kappa^2 P'_3(\nu)\frac{P_3(\mu)}{\mu} + \frac{1}{8}\kappa^4 P'_5(\nu)\frac{P_5(\mu)}{\mu} - \frac{5}{64}\kappa^6 P'_7(\nu)\frac{P_7(\mu)}{\mu} + \ldots}{1 - \frac{1}{4}\kappa^2 P'_3(\nu) + \frac{1}{8}\kappa^4 P'_5(\nu) - \frac{5}{64}\kappa^6 P'_7(\nu) + \ldots},$$
$$\kappa^2 = \frac{\alpha^2}{1+\beta^2}, \quad \nu^2 = \frac{\beta^2}{1+\beta^2} \quad \theta = \sin^{-1}\left(\frac{X}{R_a}\right), \quad \mu = \cos\theta \tag{23}$$

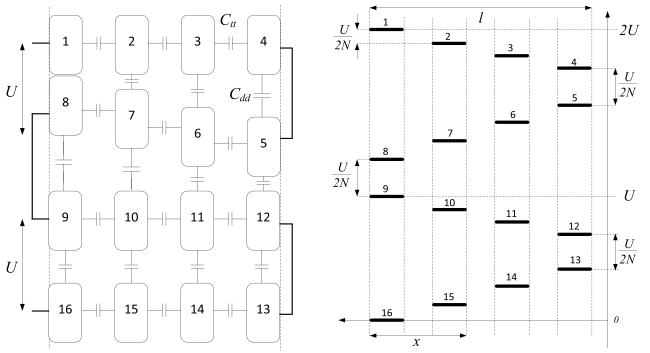

FIGURE 6. Cross-section overview and voltage distribution along deformed winding.

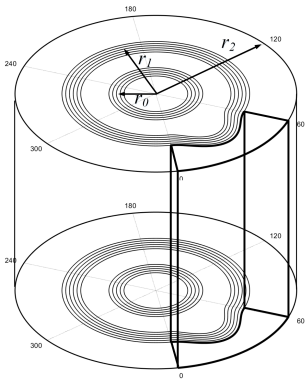

FIGURE 7. Radial deformation schematic (free-buckling).

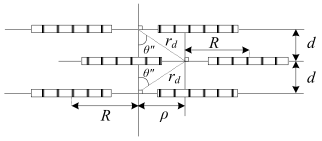

FIGURE 8. Radial displacement pattern of a disk.

B. SERIES AND SHUNT CAPACITANCES OF CIRCULAR FILAMENTS WHOSE AXES INCLINED TO ONE ANOTHER

1) SERIES CAPACITANCE

The turn-to-turn transformer winding capacitance can be influenced slightly due to the axial symmetrical and asymmetrical deformation of a winding's disk.

For the deformation illustrated in Fig. 4, equation (16) for the turn-to-turn capacitance of the second disk is obtained as:

$$C'_{tt} = \varepsilon_t \varepsilon_0 D\pi \left(\frac{h - w\tan\theta + 2\delta_t(1 - \tan\theta)}{2\delta_t} \right) \quad (28)$$

If assuming the voltage distribution along the pair of disks is uniform in our model, the inter-disk capacitance C_d will not change (see Fig. 6). Therefore, the total series capacitance in Fig. 4 will slightly reduce. This reduction is negligible as the transformer winding disks are practically close together and tan θ experiences small value. Similar calculation can be performed for Fig. 5. In Fig. 6, the cross-section overview and voltage distribution along winding is provided. The thick lines show that when moving forwards along the winding length from one conductor to the other conductor; the voltage drop over each conductor is reduced by $\Delta V = U/2N$. Each voltage level (1, 2,...) represents the voltage drop over one single turn of conductor. It also shows that the position of deformed conductors does not influence the voltage drop over the winding length.

2) SHUNT CAPACITANCE

The shunt capacitance between the winding and container (metal tank) can experience similar value in (21) as the outward parameters are still similar to the normal winding configuration.

IV. RADIAL DEFORMATION OF WINDING DISK AND ITS IMPACTS ON WINDING PARAMETERS

Radial deformation of transformer winding is modeled through free-buckling in this study. As illustrated in Fig. 7, exterior appearance of the winding shows buckling towards metal tank or it can deform towards winding center.

A. SELF- AND MUTUAL INDUCTANCES IN RADIAL DEFORMATION

The total inductance variation of a buckled winding has been discussed in [27] for conductors carrying high currents. It has been calculated and stated that the total inductance would be changed due to the buckling; however, this is potentially dependent on the deformation radius. For typical deformation in transformer winding in which deformation radius as compared to the winding radius experiences low ratio; this alteration would be insignificant. Mutual inductance variation under radial deformation of turn or filament is discussed in detail in Appendix II. It is demonstrated how this parameter can be changed due radial deformation towards the disk center or towards the metal tank.

It should be noted that the radial deformation of transformer winding is also modeled through radial displacement of a disk in some of the literatures [10] as is shown in Fig. 8.

In this case, the mutual inductance of circular elements with parallel axes is given by:

$$M''' = M_p F \quad (29)$$

where, M_p is calculated as M with a distance r_d between the disks and F is given as Table 4 in the Appendix.

Since $r_d > d$; therefore, $M_p < M$. According to Table 4, F can take a value larger or smaller than 1. Based on this and also other data in Table 4, M''' will not change significantly for the typical buckling of transformer winding particularly when θ'' is not large enough.

V. SERIES AND SHUNT CAPACITANCES IN RADIAL DEFORMATION

A. SERIES CAPACITANCE

According to (16) through (19), it can be concluded that the series capacitance including turn-to-turn and inter-disk capacitances of the buckled winding shown in Fig. 7 is

not changed significantly as the dimensions still remained unchanged for these parameters.

B. SHUNT CAPACITANCE

The electric field generated by the transformer winding is not uniform across the deformed turns. Therefore, calculation of the shunt capacitance requires the electric field determined by finite element method. This approach is considered and conducted in the next subsection through a numerical example, and the result is then compared with the analytical approach. However, for analytical discussion, if assuming a uniform electric field across the deformed section (highlighted in Fig.7), the equivalent shunt capacitance can be obtained through summation of the shunt capacitance of the normal section, C_{normal}, as given by (30) paralleled with the shunt capacitance of the deformed section, C_{deform}, as given by (31):

$$C_{normal} = \int_{(2\pi-\frac{2\pi}{\eta})}^{2\pi} \frac{\varepsilon_0 \varepsilon_r H}{\ln(\frac{r_2}{r_1})} d\phi \tag{30}$$

$$C_{deform} = \int_{0}^{2\pi/\eta} \frac{\varepsilon_0 \varepsilon_r H}{\ln\left(\frac{r_2}{r_1 - 0.5r'(\cos(\eta\phi)-1)}\right)} d\phi \tag{31}$$

where, η is the ratio of the entire trigonometric circular span (2π) over the deformation span (rad) as illustrated in Fig. 7, H is the winding height, and r' represents the deformation radius.

The total shunt capacitance of the buckled winding is eventually obtained as:

$$C'_g = C_{normal} + C_{deform} \tag{32}$$

VI. NUMERICAL EXAMPLE

A numerical example is provided to demonstrate the inductance and capacitance variation in winding deformation. It is assumed that the model winding illustrated in Fig. 1 has a single strand conductor. The radial dimension of conductor is $w = 7$ mm, axial dimension is $h = 11$ mm, inter-disk distance is $\delta_d = 6$ mm, thickness of paper insulation is $\delta_t = 0.5$ mm, relative permittivity of paper insulation is $\varepsilon_t = 3.2$, vacuum permittivity is ε_0, mean radius of winding disk is $R = 280$ mm, mean radius of the tank is $R_T = 400$ mm, and winding as well as tank height are 62 mm and 100 mm, respectively. The winding has four disks and four conductors per disk. Note that the center to center distance for pair of disks is $d = 5.5 + 5.5 + 6 = 17$ mm.

A. AXIAL DEFORMATION OF A DISK

Axial deformation of model winding is supposed to occur for the second disk. Hence, the maximum axial displacement in Fig. 4 and Fig. 5 for conductor numbered 8 would be $X = 6$ mm. Therefore, the inductance and capacitance of the model are calculated as follow using discussed analytical formulas.

1) INDUCTANCE CALCULATION

The detailed inductance matrix (μH) of the normal winding obtained is:

$L_{eq}=$

1.8221	1.3679	1.0997	0.9387	0.8500	0.9385	1.0190	1.0653	0.8128	0.7910	0.7564	0.7131	0.6006	0.6277	0.6498	0.6655
1.3679	1.7354	1.3250	1.0630	0.9066	0.9863	1.0310	1.019	0.791	0.7845	0.7631	0.7291	0.6036	0.6253	0.6409	0.6498
1.0997	1.3250	1.6507	1.284	0.9529	0.9969	0.9863	0.9385	0.7564	0.7631	0.7565	0.7354	0.6010	0.6164	0.6253	0.6277
0.9387	1.0630	1.2840	1.5682	0.9629	0.9529	0.9066	0.8500	0.7131	0.7291	0.7354	0.7287	0.5922	0.6010	0.6036	0.6006
0.8500	0.9066	0.9529	0.9629	1.5682	1.2840	1.0630	0.9385	0.8500	0.9066	0.9529	0.9629	0.7287	0.7354	0.7291	0.7131
0.9385	0.9863	0.9969	0.9529	1.2840	1.7354	1.3250	1.0997	0.9385	0.9863	0.9969	0.9529	0.7354	0.7565	0.7631	0.7564
1.019	1.0310	0.9863	0.9066	1.0630	1.3250	1.6507	1.3679	1.0190	1.0310	0.9863	0.9066	0.7291	0.7631	0.7845	0.7910
1.0653	1.019	0.9385	0.8500	0.9385	1.0997	1.3679	1.8221	1.0653	1.0997	0.9387	0.8500	0.7131	0.7564	0.7910	0.8128
0.8128	0.791	0.7564	0.7131	0.8500	0.9385	1.0190	1.0653	1.8221	1.3679	1.0997	0.9387	0.8500	0.9385	1.019	1.0653
0.791	0.7845	0.7631	0.7291	0.9066	0.9863	1.0310	1.0997	1.3679	1.7354	1.3250	1.0630	0.9066	0.9863	1.0310	1.019
0.7564	0.7631	0.7565	0.7354	0.9529	0.9969	0.9863	0.9387	1.0997	1.3250	1.6507	1.284	0.9529	0.9969	0.9863	0.9385
0.7131	0.7291	0.7354	0.7287	0.9629	0.9529	0.9066	0.8500	0.9387	1.0630	1.284	1.5682	0.9629	0.9529	0.9066	0.8500
0.6006	0.6036	0.6010	0.5922	0.7287	0.7354	0.7291	0.7131	0.8500	0.9066	0.9529	0.9629	1.5682	1.2840	1.0630	0.9387
0.6277	0.6253	0.6164	0.6010	0.7354	0.7565	0.7631	0.7564	0.9385	0.9863	0.9969	0.9529	1.2840	1.6507	1.3250	1.0997
0.6498	0.6409	0.6253	0.6036	0.7291	0.7631	0.7845	0.7910	1.019	1.0310	0.9863	0.9066	1.0630	1.3250	1.7354	1.3679
0.6655	0.6498	0.6277	0.6006	0.7131	0.7564	0.7910	0.8128	1.0653	1.0190	0.9385	0.8500	0.9387	1.0997	1.3679	1.8221

(33)

For the symmetrical axial deformation occurred on the second disk (Fig. 4), the inductance matrix is calculated as (34), while this matrix for the asymmetrical deformation (Fig. 5) is obtained as (35):

$L'_{eq}=$

1.8221	1.3679	1.0997	0.9387	0.8483	0.9365	1.0168	1.0629	0.8128	0.791	0.7564	0.7131	0.6006	0.6277	0.6498	0.6655
1.3679	1.7354	1.3250	1.0630	0.9047	0.9842	1.0287	1.0168	0.791	0.7845	0.7631	0.7291	0.6036	0.6253	0.6409	0.6498
1.0997	1.3250	1.6507	1.284	0.9508	0.9947	0.9842	0.9365	0.7564	0.7631	0.7565	0.7354	0.6010	0.6164	0.6253	0.6277
0.9387	1.0630	1.284	1.5682	0.9607	0.9508	0.9047	0.8483	0.7131	0.7291	0.7354	0.7287	0.5922	0.6010	0.6036	0.6006
0.8483	0.9047	0.9508	0.9607	1.5682	1.2840	1.0630	0.9385	0.8483	0.9047	0.9508	0.9607	0.7271	0.7338	0.7276	0.7117
0.9365	0.9842	0.9947	0.9508	1.2840	1.7354	1.3250	1.0997	0.9365	0.9842	0.9947	0.9508	0.7339	0.7548	0.7614	0.7548
1.0168	1.0287	0.9842	0.9047	1.0630	1.3250	1.6507	1.3679	1.0168	1.0287	0.9842	0.9047	0.7276	0.7614	0.7827	0.7893
1.0629	1.0168	0.9365	0.8483	0.9385	1.0997	1.3679	1.8221	1.0629	1.0168	0.9365	0.8483	0.7117	0.7548	0.7893	0.8110
0.8128	0.791	0.7564	0.7131	0.8483	0.9365	1.0168	1.0629	1.8221	1.3679	1.0997	0.9387	0.8500	0.9385	1.019	1.0653
0.791	0.7845	0.7631	0.7291	0.9047	0.9842	1.0287	1.0168	1.3679	1.7354	1.3250	1.0630	0.9066	0.9863	1.0310	1.0190
0.7564	0.7631	0.7565	0.7354	0.9508	0.9947	0.9842	0.9365	1.0997	1.3250	1.6507	1.284	0.9529	0.9969	0.9863	0.9385
0.7131	0.7291	0.7354	0.7287	0.9607	0.9508	0.9047	0.8483	0.9387	1.0630	1.284	1.5682	0.9629	0.9529	0.9066	0.8500
0.6006	0.6036	0.6010	0.5922	0.7271	0.7338	0.7276	0.7117	0.8500	0.9066	0.9529	0.9629	1.5682	1.2840	1.0630	0.9387
0.6277	0.6253	0.6164	0.6010	0.7338	0.7827	0.7614	0.7548	0.9385	0.9863	0.9969	0.9529	1.2840	1.6507	1.3250	1.0997
0.6498	0.6409	0.6253	0.6036	0.7276	0.7614	0.7548	0.7893	1.019	1.0310	0.9863	0.9066	1.0630	1.3250	1.7354	1.3679
0.6655	0.6498	0.6277	0.6006	0.7117	0.7548	0.7893	0.8110	1.0653	1.019	0.9385	0.8500	0.9387	1.0997	1.3679	1.8221

(34)

$L''_{eq}=$

1.8221	1.3679	1.0997	0.9387	0.8495	0.9380	1.0184	1.0647	0.8128	0.7910	0.7564	0.7131	0.6006	0.6277	0.6498	0.6655
1.3679	1.7354	1.3250	1.0630	0.9061	0.9857	1.0304	1.0184	0.791	0.7845	0.7631	0.7291	0.6036	0.6253	0.6409	0.6498
1.0997	1.3250	1.6507	1.2840	0.9523	0.9963	0.9857	0.9380	0.7564	0.7631	0.7565	0.7354	0.6010	0.6164	0.6253	0.6277
0.9387	1.0630	1.284	1.5682	0.9623	0.9523	0.9061	0.8495	0.7131	0.7291	0.7354	0.7287	0.5922	0.6010	0.6036	0.6006
0.8495	0.9061	0.9523	0.9623	1.5682	1.2840	1.0630	0.9385	0.8495	0.9061	0.9523	0.9623	0.8123	0.7350	0.7287	0.7127
0.9380	0.9857	0.9963	0.9523	1.2840	1.7354	1.3250	1.0997	0.9380	0.9857	0.9963	0.9523	0.7350	0.7560	0.7626	0.7560
1.0184	1.0304	0.9857	0.9061	1.0630	1.3250	1.6507	1.3679	1.0184	1.0304	0.9857	0.9061	0.7287	0.7627	0.7840	0.7905
1.0647	1.0184	0.9380	0.8495	0.9385	1.0997	1.3679	1.8221	1.0647	1.0184	0.9380	0.8495	0.7127	0.7560	0.7905	0.7283
0.8128	0.791	0.7564	0.7131	0.8495	0.9380	1.0184	1.0647	1.8221	1.3679	1.0997	0.9387	0.8500	0.9385	1.019	1.0653
0.791	0.7845	0.7631	0.7291	0.9061	0.9857	1.0304	1.0184	1.3679	1.7354	1.3250	1.0630	0.9066	0.9863	1.0310	1.0190
0.7564	0.7631	0.7565	0.7354	0.9523	0.9963	0.9857	0.9380	1.0997	1.3250	1.6507	1.284	0.9529	0.9969	0.9863	0.9385
0.7131	0.7291	0.7354	0.7287	0.9623	0.9523	0.9061	0.8495	0.9387	1.0630	1.284	1.5682	0.9629	0.9529	0.9066	0.8500
0.6006	0.6036	0.6010	0.5922	0.8123	0.7350	0.7287	0.7127	0.8500	0.9066	0.9529	0.9629	1.5682	1.2840	1.0630	0.9387
0.6277	0.6253	0.6164	0.6010	0.7350	0.7560	0.7626	0.7560	0.9385	0.9863	0.9969	0.9529	1.2840	1.6507	1.3250	1.0997
0.6498	0.6409	0.6253	0.6036	0.7287	0.7626	0.7840	0.7905	1.019	1.0310	0.9863	0.9066	1.0630	1.3250	1.6507	1.3679
0.6655	0.6498	0.6277	0.6006	0.7127	0.7560	0.7905	0.7283	1.0653	1.0190	0.9385	0.8500	0.9387	1.0997	1.3679	1.8221

(35)

As compared to (33), those elements which have changed due to the winding axial deformation are highlighted by enclosed rectangles in (34) and (35). To find these variations, (4) and (5) can be easily calculated and compared with original values in (33). The matrices in (36) and (37) give deviation values in the mutual inductance for symmetrical and asymmetrical axial deformation of one single disk in percent, respectively.

$$\Delta L'_{eq} = \begin{bmatrix} 0.00 & 0.22 & 0.00 & 0.00 \\ 0.22 & 0.00 & 0.20 & 0.21 \\ 0.00 & 0.20 & 0.00 & 0.00 \\ 0.00 & 0.21 & 0.00 & 0.00 \end{bmatrix} \tag{36}$$

$$\Delta L''_{eq} = \begin{bmatrix} 0.00 & 0.05 & 0.00 & 0.00 \\ 0.05 & 0.00 & 0.05 & 0.06 \\ 0.00 & 0.05 & 0.00 & 0.00 \\ 0.00 & 0.06 & 0.00 & 0.00 \end{bmatrix} \tag{37}$$

According to (34) and (35), the elements in M_{ab}, M_{ba}, M_{bc}, M_{cb}, M_{bd} and M_{db} are changed due to the axial deformation of the second disk. In fact, all related mutual inductances to the second disk have changed, while other elements have remained unchanged. It should be also emphasized that due to both types of axial deformation, the self-inductance of the second disk is changed slightly but it is too small to appear in the reported decimal digit numbers in 34 and 35. In addition, the variation of mutual inductances as well as the total self-inductance for symmetrical axial deformation is more as compared to the asymmetrical deformation. This in turn means that the deformation angle, θ, is quite a significant parameter in inductance variation.

2) CAPACITANCE CALCULATION

The series capacitance for the normal winding of Fig. 1 is:

$$C_s = 67.950\,pF \tag{38}$$

This value was obtained as (39) and (40) for the configurations in Fig. 4 and Fig. 5 respectively:

$$C'_s = 67.827\,pF \tag{39}$$

$$C''_s = 67.889\,pF \tag{40}$$

The shunt capacitance will remain almost constant as the outward configuration has not changed considerably.

B. RADIAL DEFORMATION ALONG THE WINDING

It is assumed that radial deformation caused part of the model winding to be stretched towards the metal tank as shown in Fig. 7, where the mean radius of deformation is $r' = \pm 50$ mm, and the deformation angle is $\varphi = \pi/2$.

In this particular case, the shunt capacitance of the winding can change significantly due to the radial deformation, while other parameters will remain almost constant. Hence, the shunt capacitance is simulated and calculated for a buckled winding similar to Fig. 7 using finite element method as well as the formulas presented in this study. The parameters of the simulated winding are same as those presented in the example (Fig. 9). Simulated and analytical results are shown in Table 1.

The results provided in Table 1 reveal that the analytical approach to calculate the shunt capacitance has reasonable accuracy in this study. However, this accuracy might not be adequate for complicated radial deformations or winding spiraling. For both finite element and analytical approaches, a winding which is bent inwards experiences less shunt capacitance than that bent outwards.

VII. CASE STUDY

Axial and radial deformations of transformer winding disk were discussed. To explore the winding disk deformation influence on FRA spectrum and determine how the inductance variation in (34) and (35) can affect the frequency response trace of transformer winding practically, a 66 kV, 25 MVA air-core isolated winding was used for axial deformation emulation.

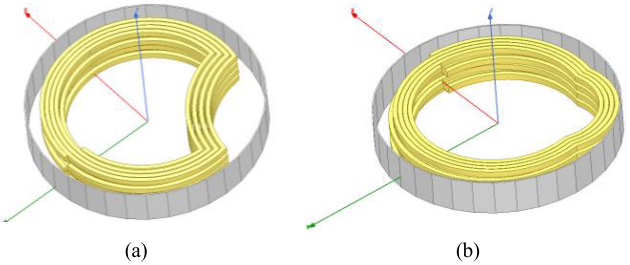

(a) (b)

FIGURE 9. The modeled winding through finite element (mean radius of winding disk = 280 mm, mean radius of tank = 400 mm, tank height = 62 mm, $r' = \pm 50$ mm, $\varphi = \pi/2$), (a) bent inwards, (b) bent outwards.

TABLE 1. Calculated capacitance between the winding and metal container (tank).

Condition	Finite Element	Analytical calculation
Normal Winding	41.461 pF	42.506 pF
Bent outwards	39.709 pF	40.325 pF
Bent inwards	67.048 pF	66.056 pF

FIGURE 10. Axially deformed winding.

This winding contains 32 disks with 24 turns per disk. At first, frequency response end-to-end open circuit measurement [28] was conducted on the original (undeformed) winding. The FRA spectrum was recorded over the frequency range of 20 Hz - 2 MHz. Afterwards, the fourth disk of the winding was tilted axially with its outermost turn shifted towards the upper disk, as shown in Fig. 10. This was achieved by inserting a plastic wedge (12 cm in height and 5 cm in base) to produce asymmetrical axial deformation. The wedge was inserted such that it influenced one half of the disk's circumference. The winding frequency response was re-recorded and the two spectra (before and after deformation) are shown in Fig. 11.

Different literatures agreed that within the FRA spectrum of single transformer winding, the first anti-resonance in the low frequency part is initiated through interaction between the winding inductive and capacitive reactance [7], [29], [30]. The case study here on this anti-resonance helps to estimate which winding's parameter has altered. Study on other frequency bands of the FRA spectrum can also narrow down the investigations, help to analyse the first anti-resonance better, and improve the diagnosis.

According to Fig.11 and moving from lower towards higher frequencies, it can be seen that the spectra in the very low-frequency region are almost matched. After around 1 kHz, the discrepancy becomes noticeable in the low-frequency band while the first anti-resonance shows FRA spectrum deviation due to the axial deformation. This in turn could be due to the inductance or shunt capacitance reduction of the winding. In addition, mid-frequency oscillations

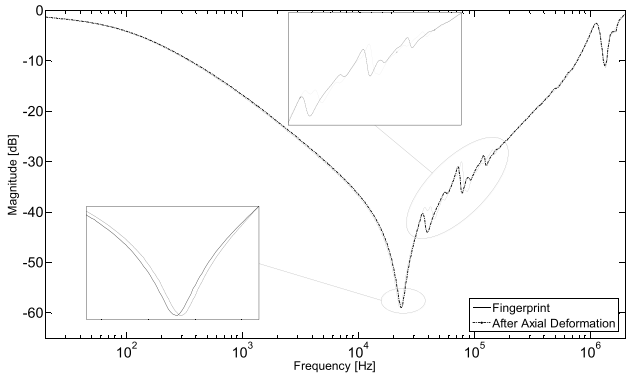

FIGURE 11. Reference and measured frequency response spectra for winding.

have altered and resonances and anti-resonances are shifted. Since the mid-frequency oscillations are initiated through the mutual inductance, series and shunt capacitances, this alteration tends to support the hypothesis that the mutual inductance or total capacitance may have been changed. Furthermore, close matching of the FRA spectra in high and very high frequency regions is indicative that deviation in spectra comes through inductance rather than capacitance variation. In fact, the low-frequency band of the FRA spectrum is mainly affected by winding inductance and deviation in this region could be due to self- or mutual inductance alteration. Hence, it can be concluded that the deviation in FRA spectrum is due to mutual inductance changes as demonstrated in the numerical example and analytical discussion. Furthermore, considering (36) and (37), it can be found that even small changes in the winding mutual inductance can influence FRA results.

VIII. CONCLUSION

Modeling of transformer windings due to radial and axial deformations is considered a significant challenge for those researchers studying transformer windings through the detailed model. To address this concern, this work focused on inductance and capacitance variations due to transformer winding disk deformation. A winding model was proposed, self- and mutual-inductances as well as series and shunt capacitances were studied in detail, and inductance and capacitance variations due to axial and radial deformations were discussed analytically. A numerical example was presented and it showed how the winding inductance value would be changed due axial tilting of a winding disk. Changes in the series capacitance value under such circumstances was not covered in detail numerically; however, it was discussed that the series capacitance variation would be insignificant in a winding disk with low impulse voltage distribution coefficient, α. Changes in the shunt capacitance value would be negligible as the outer surface winding structure remains unchanged in axial transformer winding disk tilting.

Study on radial disk deformation using the model winding revealed the shunt capacitance variation in transformer winding. It was also shown that the mutual inductance

TABLE 2. Values of *K* for single layer coil [20].

h/2R	*K*	*h/2R*	*K*	*h/2R*	*K*	*h/2R*	*K*
0	0	0.10	0.203324	0.20	0.319825	0.30	0.405269
0.01	0.034960	0.11	0.217044	0.21	0.329479	0.31	0.412650
0.02	0.061098	0.12	0.230200	0.22	0.338852	0.32	0.419856
0.03	0.083907	0.13	0.242842	0.23	0.347960	0.33	0.426890
0.04	0.104562	0.14	0.255011	0.24	0.356816	0.34	0.433762
0.05	0.123615	0.15	0.266744	0.25	0.365432	0.35	0.440474
0.06	0.141395	0.16	0.278070	0.26	0.373818	0.36	0.447036
0.07	0.158119	0.17	0.289019	0.27	0.381986	0.37	0.453450
0.08	0.173942	0.18	0.299614	0.28	0.389944	0.38	0.459724
0.09	0.188980	0.19	0.309876	0.29	0.397703	0.39	0.465860
0.10	0.203324	0.20	0.319825	0.30	0.405269	0.40	0.471865

TABLE 3. Values of *R* for inclined circles [20].

	μ	β=0	β=0.1	β=0.2		β=0	β=0.1	β=0.2
	0	0.4099	0.4741	0.6078		0.5300	0.5660	0.6550
	0.1	0.4114	0.4763	0.6095		0.5330	0.5680	0.6540
	0.2	0.4161	0.4807	0.6150		0.5360	0.5730	0.6580
	0.3	0.4229	0.4890	0.6246		0.5440	0.5780	0.6670
	0.4	0.4311	0.5012	0.6389		0.5560	0.5920	0.6800
α=0.9	0.5	0.4472	0.5185	0.6593	α=0.8	0.5730	0.6110	0.7000
	0.6	0.4673	0.5431	0.6886		0.5980	0.6330	0.7290
	0.7	0.4969	0.5794	0.7308		0.6270	0.6680	0.7650
	0.8	0.5433	0.6383	0.7951		0.6800	0.7190	0.8180
	0.9	0.6278	0.7313	0.9064		0.7640	0.8070	0.9050
	1.0	1	1	1		1	1	1
	μ	β=0	β=0.1	β=0.2		β=0	β=0.1	β=0.2
	0	0.6276	0.6498	0.7104		0.7149	0.7306	0.7746
	0.1	0.6291	0.6513	0.7121		0.7164	0.7321	0.7761
	0.2	0.6337	0.6562	0.7172		0.7209	0.7366	0.7806
	0.3	0.6420	0.6645	0.7259		0.7287	0.7444	0.7883
	0.4	0.6542	0.6769	0.7387		0.7403	0.7560	0.7996
α=0.7	0.5	0.6714	0.6943	0.7566	α=0.6	0.7563	0.7718	0.8150
	0.6	0.6950	0.7182	0.7807		0.7779	0.7932	0.8354
	0.7	0.7279	0.7512	0.8135		0.8071	0.8218	0.8621
	0.8	0.7753	0.7984	0.8585		0.8472	0.8608	0.8972
	0.9	0.8503	0.8710	0.9217		0.9055	0.9160	0.9429
	1.0	1	1	1		1	1	1

of a winding disk can be changed due to radial deformation; the extent depends on the degree of deformation and its span. Asymmetrical disk deformation was emulated in the laboratory using a 66 kV isolated winding and its frequency response spectrum was recorded. Practical measurement results showed that winding disk deformation can change the FRA spectrum. Here, the change appeared in the frequency range from 10 kHz to 200 kHz. The FRA signature over this frequency band is known to be primarily influenced by the winding inductance and shunt capacitance. However, in this particular case study, it may be initiated through the winding inductance rather than the shunt capacitance for the reason described earlier. Comparing numerical example results, (34) and (35) with deviated frequency band in Fig. 11, it can be further concluded that the change in the FRA spectrum is mainly due to mutual inductance rather than self-inductance variation.

APPENDIX I

$$P_m(\mu) = \frac{(2m-1)(2m-3)}{m!} \times \left(\mu^m - \frac{m(m-1)}{2(2m-1)}\mu^{m-2} + \frac{m(m-1)(m-2)(m-3)}{2.4(2m-1)(2m-3)}\mu^{m-4} - \ldots\right) \tag{A1}$$

$$P'_m(\nu) = \frac{m\mu P_m(\mu) - mP_{m-1}(\mu)}{\mu^2 - 1} \tag{A2}$$

TABLE 4. Values of F for parallel circles, $r_d/2R = \Lambda$, [20].

$Cos\theta^{\circ}$	Λ=1	0.9	0.8	0.7	0.6	0.5	0.4	0.3	0.2	0.1	0
0	-4.053	-1.953	-0.467	0.525	1.145	1.485	1.622	1.621	1.531	1.382	1
0.1	-1.508	-1.023	-0.168	0.550	1.055	1.357	1.495	1.513	1.448	1.327	1
0.2	-0.724	-0.387	0.117	0.585	1.010	1.264	1.392	1.421	1.376	1.278	1
0.3	-0.237	0.013	0.348	0.696	0.989	1.195	1.308	1.341	1.310	1.233	1
0.4	0.101	0.291	0.5246	0.766	0.983	1.144	1.239	1.271	1.252	1.191	1
0.5	0.351	0.493	0.658	0.829	0.984	1.105	1.181	1.211	1.199	1.153	1
0.6	0.544	0.647	0.761	0.878	0.987	1.075	1.132	1.158	1.151	1.115	1
0.7	0.695	0.766	0.842	0.920	0.991	1.050	1.091	1.111	1.108	1.085	1
0.8	0.818	0.861	0.907	0.952	0.995	1.031	1.056	1.069	1.069	1.055	1
0.9	0.917	0.937	0.958	0.979	0.998	1.014	1.026	1.032	1.033	1.026	1
1.0	1	1	1	1	1	1	1	1	1	1	1

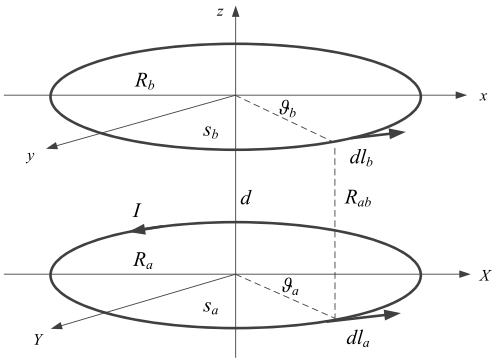

FIGURE 12. Concentric circular filaments.

APPENDIX II

A. NORMAL CONDITION

The mutual inductance between two circular filaments having radii R_a and R_b is obtained as:

$$M_{ab} = \frac{\phi_b}{I_a}, \tag{A3}$$

where ϕ_b is the induced magnetizing flux on the second loop due to the current initiated by the first loop. Hence, M_{ab} as the mutual inductance is given by:

$$M_{ab} = \oint_{c_b} A_{ab} dl_b = \frac{\mu_0}{4\pi} \oint_{c_a} \oint_{c_b} \frac{1}{R_{ab}} dl_b . dl_a$$

$$= \frac{\mu_0 R_a R_b}{4\pi} \int_0^{2\pi} \int_0^{2\pi} \frac{\cos\vartheta_a}{\left(R_a^2 + R_b^2 + d^2 - 2R_a R_b \cos\vartheta_a\right)^{1/2}} \times d\vartheta_b d\vartheta_a$$

$$\left[\text{ Note that: } R_{ab} = \left(R_a^2 + R_b^2 + d^2 - 2R_a R_b \cos\vartheta_a\right)^{1/2} \right] \tag{A4}$$

In the above, refer to Fig. 12 to find parameters and configuration It is obvious that the mutual inductance between two circular filaments is only a function of their shapes as well as orientations. This was stated in [13] and [31].

Using Maxwell's advices in [13], reference [31] discussed the solution of (A4). In fact, changing the variable ϑ_a to $2\theta''$, $\cos\vartheta_a = \cos 2\theta'' = 2\cos^2\theta'' - 1$, and $d\vartheta_a = 2d\theta''$ will

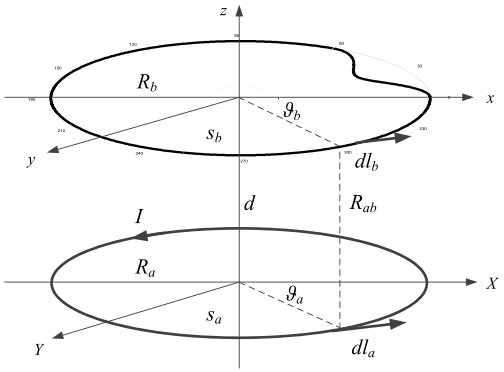

FIGURE 13. Concentric circular filaments, inward buckling demonstration for the second loop.

simplify the equation. Thus, M_{ab} can be calculated as [31]:

$$M_{ab} = \frac{\mu_0 R_a R_b}{2} \int_0^{\pi} \frac{2\cos 2\theta''}{\left((R_a+R_b)^2 + d^2 - 4R_a R_b \cos^2\theta''\right)^{1/2}} d\theta''$$

$$= \frac{\mu_0 \left(R_a R_b\right)^{1/2}}{2} \int_0^{\pi} \frac{k\cos 2\theta''}{\left(1 - k^2\cos^2\theta''\right)^{1/2}} d\theta'',$$

$$k^2 = \frac{4R_a R_b}{(R_a + R_b)^2 + d^2}$$

$$\left[\text{ Note that: } k\cos 2\theta'' = \left(\frac{2}{k} - k\right) - \frac{2}{k}\left(1 - k^2\cos^2\theta''\right) \right] \tag{A5}$$

Having information about complete elliptic integrals $K(k)$ and $E(k)$, equation (A4) is given by [13] and [31]:

$$M_{ab} = \frac{\mu_0 \left(R_a R_b\right)^{1/2}}{2} \int_0^{\pi} \frac{k\cos 2\theta''}{\left(1 - k^2\cos^2\vartheta_a\right)^{1/2}} d\theta''$$

$$= \mu_0 \left(R_a R_b\right)^{1/2} \int_0^{\pi/2} \left[\left(\frac{2}{k} - k\right) \frac{1}{\left(1 - k^2\cos^2\theta''\right)^{1/2}} - \frac{2}{k}\left(1 - k^2\cos^2\theta''\right)^{1/2} \right] d\theta''$$

$$= \mu_0 \left(R_a R_b\right)^{1/2} \int_0^{\pi/2} \left[\left(\frac{2}{k} - k\right) \frac{1}{\left(1 - k^2\sin^2\theta''\right)^{1/2}} - \frac{2}{k}\left(1 - k^2\sin^2\theta''\right)^{1/2} \right] d\theta''$$

$$= \mu_0 \left(R_a R_b\right)^{1/2} \left[\left(\frac{2}{k} - k\right) K(k) - \frac{2}{k} E(k) \right]$$

$$M'_{ab} = \frac{\mu_0 R_a}{4\pi}\int_0^{2\pi}\int_0^{2\pi/\eta} \frac{\cos\vartheta_1\left(R_b + 0.5r'(\cos\eta\vartheta_2 - 1)\right)}{\left(R_a^2 + (R_b + 0.5r'(\cos\eta\vartheta_2 - 1))^2 + d^2 - 2R_a\left(R_b + 0.5r'(\cos\eta\vartheta_2 - 1)\right)\cos\vartheta_1\right)^{1/2}} d\vartheta_2 d\vartheta_1 + \frac{\mu_0 R_a R_b}{4\pi}\int_0^{2\pi}\int_{2\pi/\eta}^{2\pi} \frac{\cos\vartheta_1}{\left(R_a^2 + R_b^2 + d^2 - 2R_a R_b\cos\vartheta_1\right)^{1/2}} d\vartheta_2 d\vartheta_1 \quad \text{(A7)}$$

where:

$$K(k) = \int_0^{\pi/2} \frac{1}{\left(1 - k^2\sin^2\theta''\right)^{1/2}} d\theta'',$$

$$E(k) = \int_0^{\pi/2} \left(1 - k^2\sin^2\theta''\right)^{1/2} d\theta'' \quad \text{(A6)}$$

Therefore, (A6) shows the analytical approach to determine the mutual inductance for concentric circular filaments.

B. MUTUAL INDUCTANCE UNDER BUCKLING

Equation (A4) is utilized to calculate the impact of buckling on the mutual inductance of two concentric circular filaments as shown in Fig. 13. It should be noted that in the case of inward buckling (Fig. 13) the winding radius for the span faced buckling is defined as $R_{bd} = R_b + 0.5r'(\cos\eta\theta - 1)$, and outward buckling (Fig. 7) is expressed as $R_{bd} = R_b - 0.5r'$ $(\cos\eta\theta - 1)$. η is the ratio of the entire trigonometric circular span (2π) over the deformed arc (in radians) as illustrated in Fig. 7, and r' represents the deformation radius.

Based on this, the mutual inductance is given by (A7), as shown at the top of this page.

where, the first part of (A7) comes through the span facing deformation and second part represents the circular part in the second filament. This integral is complex to solve analytically and better addressed numerically using software. However, to continue the equation analytically, it can be assumed that the influence of R_b (in the total value of R_{ab} as the denominator) in the first integral is negligible as compared to R_b influence as the numerator. This assumption is reasonable for the filaments which are quite far away, but perhaps it is not accurate for close loops. Having this assumption over the integrals in (A7), M'_{ab} is obtained as:

$$M'_{ab} = \frac{\mu_0 R_a}{4\pi}\int_0^{2\pi}\int_0^{2\pi/\eta} \frac{(R_b - 0.5r')\cos\vartheta_1}{\left(R_a^2 + R_b^2 + d^2 - 2R_a R_b\cos\vartheta_1\right)^{1/2}} \times d\vartheta_2 d\vartheta_1 + \frac{\mu_0 R_a}{4\pi}\int_0^{2\pi}\int_0^{2\pi/\eta} \frac{0.5r'\cos\vartheta_1\cos\eta\vartheta_2}{\left(R_a^2 + R_b^2 + d^2 - 2R_a R_b\cos\vartheta_1\right)^{1/2}} \times d\vartheta_2 d\vartheta_1 + \frac{\mu_0 R_a R_b 2\pi(1 - \eta^{-1})}{4\pi} \times \int_0^{2\pi} \frac{\cos\vartheta_1}{\left(R_a^2 + R_b^2 + d^2 - 2R_a R_b\cos\vartheta_1\right)^{1/2}} d\vartheta_1 \quad \text{(A8)}$$

where the first integral in (A7) has been split in (A8). Upon integrating one step, M'_{ab} is given by:

$$M'_{ab} = \frac{\mu_0 R_a(R_b - 0.5r')}{2\eta} \times \int_0^{2\pi} \frac{\cos\vartheta_1}{\left(R_a^2 + R_b^2 + d^2 - 2R_a R_b\cos\vartheta_1\right)^{1/2}} d\vartheta_1 + \frac{\mu_0 R_a r'}{8\pi\eta}\int_0^{2\pi} \frac{\cos\vartheta_1}{\left(R_a^2 + R_b^2 + d^2 - 2R_a R_b\cos\vartheta_1\right)^{1/2}} d\vartheta_1 + \frac{\mu_0 R_a R_b(1 - \eta^{-1})}{2} \times \int_0^{2\pi} \frac{\cos\vartheta_1}{\left(R_a^2 + R_b^2 + d^2 - 2R_a R_b\cos\vartheta_1\right)^{1/2}} d\vartheta_1 \quad \text{(A9)}$$

After simplification of (A9), M'_{ab} is obtained as:

$$M'_{ab} = \left(\frac{\mu_0 R_a r'(1 - 2\pi)}{8\pi\eta} + \frac{\mu_0 R_a R_b}{2}\right)\int_0^{2\pi} \times \frac{\cos\vartheta_1}{\left(R_a^2 + R_b^2 + d^2 - 2R_a R_b\cos\vartheta_1\right)^{1/2}} d\vartheta_1 \quad \text{(A10)}$$

Comparing (A10) with (A5), it is obvious that the term having $(1-2\pi)$ slightly reduces the mutual inductance within inward buckling as it takes a negative value. Accordingly, this coefficient will change to a positive value $(1 + 2\pi)$ when the outward buckling occurred for the filament (see Fig.7).

REFERENCES

[1] M. M. F. Yousof, C. Ekanayake, and T. K. Saha, "Frequency response analysis to investigate deformation of transformer winding," *IEEE Trans. Dielectr. Electr. Insul.*, vol. 22, no. 4, pp. 2359–2367, Aug. 2015.

[2] M. Florkowski, J. Furgal, and P. Pajak, "Analysis of fast transient voltage distributions in transformer windings under different insulation conditions," *IEEE Trans. Dielectr. Electr. Insul.*, vol. 19, no. 6, pp. 1991–1998, Dec. 2012.

[3] K. Ludwikowski, K. Siodla, and W. Ziomek, "Investigation of transformer model winding deformation using sweep frequency response analysis," *IEEE Trans. Dielectr. Electr. Insul.*, vol. 19, no. 6, pp. 1957–1961, Dec. 2012.

[4] N. Abeywickrama, Y. V. Serdyuk, and S. M. Gubanski, "Effect of core magnetization on frequency response analysis (FRA) of power transformers," *IEEE Trans. Power Del.*, vol. 23, no. 3, pp. 1432–1438, Jul. 2008.

[5] V. Behjat, A. Vahedi, A. Setayeshmehr, H. Borsi, and E. Gockenbach, "Diagnosing shorted turns on the windings of power transformers based upon online FRA using capacitive and inductive couplings," *IEEE Trans. Power Del.*, vol. 26, no. 4, pp. 2123–2133, Oct. 2011.

[6] S. D. Mitchell and J. S. Welsh, "Methodology to locate and quantify radial winding deformation in power transformers," *IET High Voltage*, vol. 2, no. 1, pp. 17–24, 2016.
[7] M. Bagheri, M. S. Naderi, and T. Blackburn, "Advanced transformer winding deformation diagnosis: Moving from off-line to on-line," *IEEE Trans. Dielectr. Electr. Insul.*, vol. 19, no. 6, pp. 1860–1870, Dec. 2012.
[8] E. Gomez-Luna, G. A. Mayor, C. Gonzalez-Garcia, and J. P. Guerra, "Current status and future trends in frequency-response analysis with a transformer in service," *IEEE Trans. Power Del.*, vol. 28, no. 2, pp. 1024–1031, Apr. 2013.
[9] K. G. N. B. Abeywickrama, Y. V. Serdyuk, and S. M. Gubanski, "Exploring possibilities for characterization of power transformer insulation by frequency response analysis (FRA)," *IEEE Trans. Power Del.*, vol. 21, no. 3, pp. 1375–1382, Jul. 2006.
[10] E. Rahimpour, M. Jabbari, and S. Tenbohlen, "Mathematical comparison methods to assess transfer functions of transformers to detect different types of mechanical faults," *IEEE Trans. Power Del.*, vol. 25, no. 4, pp. 2544–2555, Oct. 2010.
[11] A. Abu-Siada, N. Hashemnia, S. Islam, and M. A. S. Masoum, "Understanding power transformer frequency response analysis signatures," *IEEE Elect. Insul. Mag.*, vol. 29, no. 3, pp. 48–56, May 2013.
[12] H. Tarimoradi and G. B. Gharehpetian, "Novel calculation method of indices to improve classification of transformer winding fault type, location, and extent," *IEEE Trans. Ind. Informat.*, vol. 13, no. 4, pp. 1531–1540, Aug. 2017.
[13] J. C. Maxwell, *A Treatise on Electricity and Magnetism*, vol. 2, 3rd ed. Oxford, U.K.: Clarendon, 1892, pp. 334–339, sec. 696–701.
[14] L. Rayleigh, "Self-induction of electric currents in a thin anchorring," *Proc. Roy. Soc.*, vol. 86, no. 590, pp. 562–571, Jun. 1912, doi: 10.1098/rspa.1912.0046.
[15] T. R. Lyle, "On circular filaments or circular magnetic shells equivalent to circular coils, and on the equivalent radius of a coil," *London, Edinburgh, Dublin Philosophical Mag. J. Sci.*, vol. 3, no. 15, p. 310, 1902.
[16] S. Butterworth, "On the coefficients of mutual induction of eccentric coils," *London, Edinburgh, Dublin Philosophical Mag. J. Sci.*, vol. 31, no. 185, pp. 443–454, 1916.
[17] C. Snow, *Formulas for Computing Capacitance and Inductance*, Standard 544, National Bureau Standards Circular, Washington, DC, USA, Dec. 1954.
[18] E. B. Rosa, "Calculation of the self-inductance of single-layer coils," *Bureau Standards Bull.*, vol. 2, pp. 161–187, Jul. 1906.
[19] H. L. Curtise and M. C. Sparks, "Formulas, tables and curves for computing the mutual inductance of two coaxial circles," *Bureau Standards Bulletin*, vol. 19, no. 492, pp. 541–576, 1924.
[20] F. W. Grover, *Inductance Calculations: Working Formulas and Tables*. New York, NY, USA: Dover, 1962.
[21] S. Babic, F. Sirois, C. Akyel, and C. Girardi, "Mutual inductance calculation between circular filaments arbitrarily positioned in space: Alternative to Grover's formula," *IEEE Trans. Magn.*, vol. 46, no. 9, pp. 3591–3600, Sep. 2010.
[22] J. T. Conway, "Inductance calculations for non-coaxial coils using Bessel functions," *IEEE Trans. Magn.*, vol. 43, no. 3, pp. 1023–1034, Mar. 2007.
[23] G. Kirchhoff, *Gesammelte Abhandlungen*. Leipzig, Germany: J. A. Barth, 1882, p. 177.
[24] H. Nagaoka, "The inductance coefficient of solenoids," *J. Colloids Sci. Tokyo*, vol. 27, Mar. 1909, Art. no. 6.
[25] F. W. Grover, *Additions to the Formulas for the Calculation of Mutual and Self-Inductance*, vol. 14. Bulletin of the Bureau Standards, 1919, paper 169. [Online]. Available: http://dx.doi.org/10.6028/bulletin.348
[26] K. Karsai, D. Kerenyi, *Large Power Transformer*. New York, NY, USA: Elsevier, 1987, pp. 187–214.
[27] S. Chattopadhyay, "Buckling behavior of a superconducting magnet coil," *Int. J. Solids Struct.*, vol. 43, no. 17, pp. 5158–5167, 2006.
[28] *Measurement of Frequency Response, Ed. 1.0*, IEC Standard 60076-18, 2012.
[29] S. A. Ryder, "Diagnosing transformer faults using frequency response analysis," *IEEE Elect. Insul. Mag.*, vol. 19, no. 2, pp. 16–22, Mar. 2003.
[30] Z. Wang, J. Li, and D. M. Sofian, "Interpretation of transformer FRA responses—Part I: Influence of winding structure," *IEEE Trans. Power Del.*, vol. 24, no. 2, pp. 703–710, Feb. 2009.
[31] C. R. Paul, *Inductance Loops and Partial*, 1st ed. Hoboken, NJ, USA: Wiley, 2009.

MEHDI BAGHERI (M'12) received the M.Sc. degree in power engineering from the Sharif University of Technology, Tehran, Iran, in 2007. He joined the Iran Transformer Research Institute, Tehran as a Research Engineer, and was Head of the Test and Diagnostic Department from 2008 to 2010. In 2014, he received the Ph.D. degree from the University of New South Wales, Sydney, Australia. From 2015 to 2016, he served as the Post-Doctoral Research Fellow with the Electrical Engineering Department, National University of Singapore, involved closely with Rolls-Royce Pte. Ltd. On condition monitoring and predictive maintenance of marine transformers and filters. He is currently an Assistant Professor with the School of Electrical and Electronic Engineering, University of Nazarbayev, Astana, Kazakhstan. He is currently a member of the IEEE Dielectrics and Electrical Insulation Society. His research interests include field and marine applications of high-voltage engineering, condition monitoring, and diagnosis of power transformers and electrical rotating machines, transients in power systems and power quality.

SVYATOSLAV NEZHIVENKO received the bachelor's degree in power engineering from the Karaganda State Technical University, Karaganda, Kazakhstan, in 2009, and the M.Sc. degree in electrical and computer engineering from the University of British Columbia, Canada, in 2014. He is currently pursuing the Ph.D. degree in power engineering with Nazarbayev University. He has been the Head of Communication Department, Astana Power Plant, in 2015. His research interest includes high voltage, transformer monitoring and diagnosis.

B. T. PHUNG (M'87–SM'12) received the Ph.D. degree in electrical engineering from the University of New South Wales (UNSW), Sydney, Australia, in 1998. He is currently an Associate Professor with the School of Electrical Engineering, UNSW. He has over 30 years of practical research/development experience in partial discharge measurement and analysis, and in on-line condition monitoring of high-voltage equipment. Much of his research has involved collaborative projects between UNSW and Australian power utilities. His research interests include electrical insulation (dielectric materials and diagnostic methods), high-voltage engineering (generation, testing and measurement techniques), electromagnetic transients in power systems, and power system equipment (design and condition monitoring methods).

TREVOR BLACKBURN is currently with the School of Electrical Engineering and Telecommunications, University of New South Wales. His research interests are in power equipment condition monitoring and gas discharges, particularly in the partial discharge monitoring and lightning applications. He is a member of a number of CIGRE working groups.